Title
CPG Control for Harmonic Motion of Assistive Robot With Human Motor Control Identification

Journal
IEEE Transactions on Control Systems Technology, 28(4)

ISSN
1063-6536

Authors
Zhao, Jinxin
Iwasaki, Tetsuya

Publication Date
2020-07-01

DOI
10.1109/tcst.2019.2910160

Peer reviewed

CPG Control for Harmonic Motion of Assistive Robot with Human Motor Control Identification

Jinxin Zhao and Tetsuya Iwasaki

Abstract— **Various movements in human life, such as walking, bicycling, cleaning, chewing, swimming, etc., are periodic or repetitive. This paper proposes a method for designing a feedback controller for a robotic system to help a human with periodic (harmonic, in particular) motion tasks. The control objective is to stabilize a human-intended oscillatory movement while reducing the required human effort. For the control architecture, we adopt the central pattern generator (CPG), which is a neuronal circuit for rhythmic motor pattern. Animal locomotions under CPG control are capable of complying with various environment dynamics to yield different oscillatory movements. We take advantage of this adaptation property of the CPG controller that acts as a nonlinear damping compensator and removes part of the resistive forces in the system, thereby reducing the human effort without interfering with the human intention. It is shown that the resulting human-intended oscillation is a locally stable harmonic solution of the closed-loop human-robot-CPG system, assuming a simple model of the human motor control. The proposed control method is experimentally validated for a simple robotic arm, with a system identification of the human motor control.**

I. Introduction

Repetitive body movements, such as the swing motion of legs and arms during human locomotion, are essential in human life. Inventions of mechanical devices that help human achieve those movements (e.g., exoskeleton) would be of significant benefit to the human with disability due to aging, injury, neurological disorder, etc. Human assistive system has drawn decent amount of attention from robotics researchers. This kind of devices can provide assistive forces to the operator, thereby reducing his/her effort and stabilizing the desired oscillatory movements. Studies e.g. [1], [2] have shown that such devices can be used for neuro-rehabilitation to improve motor control capability.

Control algorithms for human assistive devices have been studied and some effective methods are proposed. The most commonly-used control strategy in assistive device is a combination of predefined trajectory with impedance control [3]. For a lower limb orthosis called ATLAS [4], the gait pattern is first analyzed and pre-generated, then a passive PD controller regulates the actual movement to the pre-defined trajectory through a restoring force emulating a mechanical impedance. A similar approach is used in robot suit HAL [2], where the reference gait pattern is generated off-line, the human intended walking phase is estimated in real time to generate a command signal, and then a PD controller achieves the regulation. Another control method, admittance control, is often employed to provide assistive power for large payload, where the controllers modify the apparent payload felt by the human through force feedback [5], [6].

A major challenge for controlling assistive devices is the detection of the human intention. A seminal work [7] is based on measured electromyography (EMG) signals, which indicate the electrical activity of skeletal muscles. Such signals can be used as an explicit indication of human intention. The detected EMG signal is passed through a Hill-type muscle model to estimate the intended joint moment, which is then used as a reference command for a moment servo controller to drive an exoskeleton. This powerful technique provides numerous possibilities in clinical/biomedical applications for assisting humans; see e.g. [8]. However, EMG signals may not perfectly correlate with human intention without careful calibrations due to the complex musculoskeletal structure and activation dynamics. Other methods for detecting human intention, in addition to EMG signals, include the direct sensing of the forces applied by the human [9], and electroencephalogram (EEG) signals [10]. While these methods have been shown to be effective to some extent, none of these is accepted as the best and ongoing researches still seek for improved methods.

Most existing methods for controlling human assistive devices apply to general, possibly non-repetitive movement tasks. When we consider periodic motions such as walking, however, we can exploit biological knowledge at the neuronal level for developing control algorithms. Neuroscience researches have shown that periodic body movements in animal locomotion are controlled by neuronal circuits called the central pattern generators (CPGs), which are nonlinear oscillators producing rhythmic pattern outputs for commanding muscle contractions [11]. The CPG mechanisms in [12] have been adopted for walking rehabilitation to generate reference trajectories of kinematic variables, modulated by EEG signals indicating the gait cycle phase [10]. Similar approaches have been taken for walking assistance by exoskeletons using adaptive frequency oscillators with encoder feedback [13], [14], and phase estimators based on position and ground force measurements [15]. Other approaches include [16], where the Hopf oscillator is exploited for controlling a robotic arm to shake hands with human using force feedback.

While the CPG-based approaches mentioned above employ explicit learning mechanisms for adapting the CPG parameters to kinematic motion variables, the CPG has an ability, without such parameter adaptation, to comply with varying environmental dynamics through sensory feedback [17]. In particular, a CPG can detect the resonance frequency of a mechanical system through position measurements and achieve a natural mode of oscillation as a stable limit cycle of the closed-loop

This work is supported by NSF grant no.1427313. The authors gratefully acknowledge helpful discussions with Jacob Rosen at UCLA.

Jinxin Zhao and Tetsuya Iwasaki are with the Department of Mechanical and Aerospace Engineering, University of California, Los Angeles, California. Email: {jinxinzh,tiwasaki}@ucla.edu.

control system [18]–[20]. If we view the human action as shaping of the natural dynamics, the CPG mechanisms appear to be useful for assistive control by complying with human intention. However, whether this idea works or not depends on the dynamics of human motor control.

Understanding how human chooses the motor control command would provide a guidance for helping impaired patients to regain certain motor capability, as well as for designing assistive and rehabilitation devices. To explain the visual-guided reaching movement mechanism, different models have been proposed, including feedforward, feedback, and hybrid models, and there has been an ongoing controversy among these three models [21]. The feedforward model suggests that human motor command is pre-planned based on the target and initial states, while fine adjustment through feedback only happens during the end of the task [22], [23]. The feedback model assumes that the muscle command is produced during the movement based on the difference between target and current states [24], [25]. An improved feedback model is discussed in [26], where an inner observer is added to the control loop. The hybrid model combines the feedforward and feedback model, and a validation of such model has been conducted in [21]. As described in [27], the feedforward part of a hybrid model can be learned by a neural network.

In this paper, we examine the ability of a CPG control, without explicit learning mechanisms, to drive a mechanical system interacting with a human, and assist with oscillatory movement tasks. We adopt the reciprocal inhibition oscillator (RIO) for the control architecture, which is a simple and well-studied type of CPG. We consider the situation where a human applies a force to a single degree-of-freedom (DOF) robotic system, loaded by a resistive environment, to achieve an intended harmonic motion. A design problem is formulated for the RIO control to drive the system and stabilize the human-intended oscillation, while reducing the human burden.

Motivated by the mechanism of the RIO to achieve robust entrainment to a natural oscillation [18], [20], we first derive a condition for the RIO controller to achieve a damping compensation approximately. The nonlinear closed-loop robot-RIO-human system is then analyzed to give a sufficient condition for stability of the human-intended harmonic motion, assuming that the human motor control can be modeled as a combination of feedforward and feedback terms. The model-based analysis has shown that the control design does not require precise knowledge of the human model, and the stability is guaranteed if the human control satisfies a certain qualitative property. This has lead to a design procedure that is essentially model-free. Moreover, unlike most of the existing CPG-based methods mentioned earlier, our RIO control is simple due to the lack of explicit mechanisms for detecting the human intention, and has a rigorous theoretical guarantee of convergence to the human-intended oscillation under a certain assumption on the human control model, which is experimentally validated.

The proposed RIO control scheme is validated through physical experiments on a simple robotic arm. We first perform a system identification for the human motor control under various loading conditions, and examine plausibility of the hybrid human control model and satisfaction of the stability condition. We then design a CPG-based assistive controller and demonstrate its performance in reducing the human effort.

Preliminary results of this article on the theoretical aspect were presented at a conference [28], where the proofs were omitted and the design method was illustrated by numerical examples. Here, all the results are rigorously proven and human-robot experiments are conducted to validate the assumption on the human motor control and demonstrate the performance of the controller.

II. CPG Assistive Control Theory

A. Problem Formulation

We consider a situation where a human is tasked to achieve a repetitive movement $z = z_d$ of a loaded object by applying a force input v as shown in Fig. 1a, where z and z_d are the displacement of the object and the desired trajectory, respectively. Suppose a mechanical device, labeled as "Mech" in Fig. 1b, is constructed and coupled to the load to help the human with the task. Our objective is to develop a systematic method for designing a feedback controller, labeled as "CPG" in Fig. 1b, that assists the human by applying a force input u through the device based on its displacement y so that the human-intended periodic motion is achieved while the human control effort is reduced. We will formalize the problem and provide a theoretically justified solution, using the one-DOF mechanical system.

Assume that the load is of resistive nature, and the force $v_\ell(t)$ required to make its displacement $z(t) \in \mathbb{R}$ is modeled by $v_\ell = d_\ell \dot{z}$ with a damping coefficient $d_\ell \in \mathbb{R}$. The mechanical device is rigidly coupled with the load so that they share the same displacement $y = z$. The dynamics of the coupled system are described by

$$m\ddot{z} + d\dot{z} + kz = v + u \tag{1}$$

where $m, c, k \in \mathbb{R}$ are the mass, damping and stiffness of the device, $d := c + d_\ell$ is the damping coefficient containing the effects of both device and load, $v(t) \in \mathbb{R}$ and $u(t) \in \mathbb{R}$ are the force inputs from a human and an actuator driven by a feedback controller, and $z(t) \in \mathbb{R}$ is the resulting displacement.

Suppose the human intends to achieve an oscillatory movement

$$z_d(t) = a_d \sin \omega_d t. \tag{2}$$

Without help from the controller ($u = 0$), the human input must satisfy $v = v_o$ when achieving $z = z_d$, where

$$v_o := m\ddot{z}_d + d\dot{z}_d + kz_d. \tag{3}$$

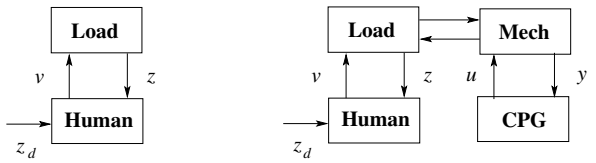

(a) Without assistive control (b) With assistive control

Fig. 1: Human operation with/without assistive control

This force input v_o would require more human effort than the original load force v_ℓ due to the added mechanical impedance of the assistive device. However, the idea is to generate a periodic assistive force $u = u_d$ in the steady state through a controller so that the force required by the human $v = v_d$ is smaller in magnitude than v_ℓ, where $v_d := v_o - u_d$.

The human burden may be reduced by a simple damping compensator $u = \delta \dot{z}$. With this control, the steady state input from the human should be $v = v_d$ where

$$v_d = m\ddot{z}_d + (d - \delta)\dot{z}_d + kz_d.$$

It can readily be shown that[1]

$$\|v_\ell\|_\infty^2 - \|v_d\|_\infty^2 = (a_d\omega_d)^2\Big(d_\ell^2 - (d-\delta)^2\Big) - a_d^2(k - m\omega_d^2)^2.$$

Thus the human effort as measured by the amplitude of input force would be reduced if the amount of damping compensation δ is close to the system damping d, provided the resistive load dominates the inertia and stiffness effects of the device, i.e.

$$\|v_\ell\|_\infty > \|v_d\|_\infty \quad \text{if} \quad d_\ell > \sqrt{|k/\omega_d^2 - m|}, \quad \delta \cong d. \tag{4}$$

If the operating frequency ω_d is roughly known and fixed *a priori*, then the device may be designed to have a natural frequency $\sqrt{k/m}$ close to ω_d so that the load-dominance condition is satisfied. If ω_d is uncertain and/or varying from one operation to another, m and k of the device may be virtually set small by a minor feedback control.

However, the linear damping compensation $u = \delta \dot{z}$ with $\delta = d$ would make the augmented plant, seen by the human, marginally stable, and a small perturbation of d could destabilize the controlled plant. In this case, the burden of stabilization is on the human control, requiring an extra human effort.

We consider a nonlinear feedback controller of the form

$$u = \mathsf{g}(p), \quad \dot{p} = \mathsf{h}(p, z), \tag{5}$$

that generates input u based on measured output z, where g and h are functions to be designed and $p(t)$ is the controller state vector. Let $(u, p) = (u_d, p_d)$ be the periodic solution to (5) when it is driven by $z = z_d$. We aim to design the controller so that the human burden is reduced in terms of not only the magnitude of the human force $v_d := v_o - u_d$ during the steady state oscillation $z = z_d$ but also the effort $v - v_d$ during the transient to stabilize the desired oscillation z_d.

One of the design criteria is to achieve approximate damping compensation $u_d \cong \delta \dot{z}_d$ with a specified amount δ to reduce the human effort in the steady state as described in (4). Another criterion, roughly speaking, is to maintain stability felt by the human even when δ is perturbed from the true value d. To explain the idea, consider the augmented closed-loop system of mechanical plant (1) and controller (5), which receives human input v and produces output z. If a fixed open-loop control input $v = v_d$ by the human yields the output z converging to z_d, then the human would feel stability and find it easy to achieve the target oscillation. If the open-loop input $v = v_d$ results in diverging output z, then the human would feel instability and has to add feedback correction terms to make z converge to z_d. Thus, we aim to maintain robust stability of the augmented system against perturbations in the amount of damping compensation δ. Note, however, that the stability property should be required not for the equilibrium at the origin but for the target oscillation z_d.

To formalize the stability requirement for the control design, let us introduce a particular model of the human motor control. Various models have been proposed in the literature, including feedforward, feedback, and hybrid models, and there has been an ongoing controversy among these three models [21], [29], [30] A general form that can represent all these models in our context is given by $v = v_d + f(z, z_d)$, where the feedforward signal $v_d(t)$ is the force required to achieve the target motion z_d, and the feedback function $f(z, z_d)$ (which is possibly dynamic) should vanish on the target trajectory, i.e. $f(z_d, z_d) = 0$. Assuming the linear state feedback, we use

$$v = v_d + \alpha(\dot{z} - \dot{z}_d) + \beta(z - z_d), \tag{6}$$

where α and β are constant gains. With the control input $u = u_d$, the feedforward term should be given by $v_d = v_o - u_d$ so that the target oscillation $z = z_d$ is a solution to the closed-loop system defined by (1), (5), and (6). Although (6) involves v_o and u_d, it does not mean that the human is explicitly conscious of the values of these signals. The human just decides how much force v to apply, based on the current z relative to the intended oscillation z_d, trying to match z with z_d. As a result, the human input v is necessarily equal to the feedforward term v_d once the convergence of z to z_d is achieved.

The problem addressed in this paper can now be formally stated as follows.

Problem 1: Consider the mechanical system in (1) and let a desired oscillation be given by (2).

(a) Design a controller (5) such that a periodic response $(u, p) = (u_d, p_d)$ to $z = z_d$ gives an approximate damping compensation $u_d \cong \delta \dot{z}_d$ with a prescribed value of δ.

(b) Analyze the closed-loop system of (1) and (5) with additional human control (6), and determine the condition for the periodic solution $(p, z, \dot{z}) = (p_d, z_d, \dot{z}_d)$ to be stable.[2]

In the next section, we will characterize a class of nonlinear controllers that approximately achieve $u = \delta \dot{z}$. A condition on the controller parameters will then be given to guarantee stability of the desired oscillation z_d in the section that follows.

Note that we do not require the human model for the control design in Problem 1(a). The stability condition in Problem 1(b) will be developed for the particular human model in (6), which would not exactly reflect the reality. Nevertheless, the result will help us develop an expectation of when the controller will be effective and will guide the design process. The validity of the human model and effectiveness of the control design will be demonstrated by experiments later in Section III.

[1]The infinity norm is defined by $\|x\|_\infty := \sup_t \|x(t)\|$.

[2]A solution $x = x_d$ of a dynamical system $\dot{x} = f(x, t)$ is said to be stable if $\|x(t) - x_d(t)\|$ converges to zero as time t goes to infinity whenever the initial deviation $\|x(0) - x_d(0)\|$ is sufficiently small.

B. CPG Control for Damping Compensation

For the architecture of controller (5), we adopt a rather simple and well-studied CPG, called the reciprocal inhibition oscillator (RIO). A mathematical description of the RIO controller is given by (see [18], [19])

$$q = b(s)(L\Psi(q) + Hz), \quad u = G\Psi(q), \tag{7}$$

with $q(t) \in \mathbb{R}^2$ being the variable, and

$$b(s) = \frac{2\varpi s}{(s+\varpi)^2}, \quad l = \begin{bmatrix} 1 \\ -1 \end{bmatrix}, \quad \begin{matrix} G = gl^{\mathsf{T}}, \\ H = hl, \end{matrix} \tag{8}$$

$$\Psi(q) = \begin{bmatrix} \psi(q_1) \\ \psi(q_2) \end{bmatrix}, \quad L = -\mu \begin{bmatrix} 0 & 1 \\ 1 & 0 \end{bmatrix},$$

where $g, h, \mu, \varpi \in \mathbb{R}$ are design parameters, $\psi(x)$ is a sigmoid (bounded, increasing, odd) function capturing the synaptic threshold effect, and $b(s)$ is a band-pass filter representing the time lag and adaptation in neuronal dynamics. The parameters μ and ϖ are assumed positive, and we use $\psi(x) := \tanh(x)$. The RIO exhibits anti-phase oscillations of q_1 and q_2 with a frequency near ϖ in the absence of input ($z = 0$) when the coupling strength is sufficiently large ($\mu > 1$). With an arbitrary input z and an arbitrary initial condition, it is proven [19] that the anti-phase property is preserved in the steady state, i.e., $q_1 + q_2$ converges to zero as $t \to \infty$.

In what follows, we will derive a condition under which the RIO control in (7) compensates for the damping so that $u \cong \delta\dot{z}$ for a fixed parameter δ, where the equality holds only approximately due to the nonlinearity in (7). A classical tool for approximating a static nonlinearity in the context of oscillation analysis is the describing function [31]. While describing functions provide fairly accurate predictions of oscillatory behaviors [32], it is difficult to guarantee dynamical properties with proofs when they are used for analyses. Here we propose another approximation method that turns out later to allow for a rigorous stability analysis. In particular, for a T-periodic signal $x(t)$, we approximate $\psi(x)$ using the average slope:

$$\psi(x) \cong \kappa(x)x, \quad \kappa(x) := \frac{1}{T}\int_0^T \psi'(x(t))dt$$

where ψ' is the derivative of ψ.

Now, consider the control input u generated by a T-periodic input z through (7), where we assume that q and u are also T-periodic. The existence of a periodic solution q to (7) can be justified by Lemma 2 in the appendix when $|h|$ is sufficiently small. Since $q_1 + q_2 = 0$ in the steady state [19], q can be expressed as $q = xl$ for some T-periodic signal $x(t) \in \mathbb{R}$. Since ψ is an odd function, we also have $\Psi(q) = \psi(x)l$. Substituting $q = xl$ and $\Psi(q) = \psi(x)l$, and noting that $Gl = 2g$ and $Ll = \mu l$, the dynamical relationship in (7) reduces to

$$u = 2g\psi(x), \quad x = b(s)(\mu\psi(x) + hz).$$

To obtain a linear approximation of the system near the target oscillation $z = z_d$, let x_d be the solution to the above equation when the input to the controller is $z = z_d$. Employing the average slope method, $\psi(x)$ can be approximated as $\psi(x) \cong \kappa(x_d)x$ in the neighborhood of $x = x_d$. In this case, the RIO control in (7) is approximately given by

$$u \cong K(s)z, \quad K(s) := \frac{2gh\kappa(x_d)b(s)}{1 - b(s)\mu\kappa(x_d)}. \tag{9}$$

The following result gives a condition for this approximate controller to compensate for the damping.

Theorem 1: Consider the RIO control (7). Let $\delta \in \mathbb{R}$ be a positive scalar and $z_d(t)$ be given by (2). Suppose there exists a T-periodic solution $x_d(t)$ to

$$x_d = b(s)(\mu\psi(x_d) + hz_d) \tag{10}$$

where $T = 2\pi/\omega_d$, and define $K(s)$ as in (9). Then, the RIO control achieves the damping compensation approximately, i.e., $K(s) = \delta s$ for $s = j\omega_d$, if and only if

$$\frac{4gh\varpi\kappa(x_d)}{\varpi^2 - \omega_d^2} = \delta, \tag{11a}$$

$$\mu\kappa(x_d) = 1, \tag{11b}$$

are satisfied.

Proof: The result follows by noting that

$$K(s) = \frac{4gh\varpi\kappa(x_d)s}{s^2 + 2\varpi(1 - \mu\kappa(x_d))s + \varpi^2} \tag{12}$$

and verifying that $K(j\omega_d) = j\omega_d\delta$ is equivalent to (11). ■

Lemma 2 in the appendix guarantees the existence of T-periodic x_d satisfying (10) when $|h| \neq 0$ is sufficiently small and $\mu \neq 1$. In this case, $q_d := x_d l$ is a solution to (5) with $z = z_d$, and the corresponding control input u is well defined. Theorem 1 characterizes the parameters of the RIO control such that the damping compensation $u = \delta\dot{z}$ is achieved approximately near the target operating condition $z = z_d$, thereby reducing the human effort. A benefit of the nonlinear RIO controller over the simple linear compensation $u = \delta\dot{z}$ is the stability felt by the human. With the linear control, the closed-loop system of (1) and $u = \delta\dot{z}$, which receives the human force v as the input, is stable when $\delta < d$ but becomes unstable when $\delta > d$. With the RIO control, however, the free response of the closed-loop system of (1) and (7) is convergent for both cases. The stability properties are illustrated by the initial state responses simulated with $v = 0$ in Fig. 2, where the system parameters are fixed, using Theorem 1, to

$$\begin{matrix} (m, d, k) = (1, 10, 2), & \omega_d = 1, \\ (h, \mu, \varpi) = (0.5, 1.01, 5), & g = \delta\mu(\varpi^2 - \omega_d^2)/(4h\varpi), \end{matrix}$$

with two cases of damping compensation $\delta = 11$ and 9 (the blue curve for the case $\delta = 11$ plots $z/100$ to show the divergence behavior). Note that g depends on the other controller parameters (δ, μ, ϖ, h) and the frequency ω_d of the target oscillation, but is independent of the model parameters of the mechanical plant and the human motor control. More importantly, g is proportional to δ, and hence with the stability, the value of the gain g in the RIO control can be safely and directly tuned on the experimental site to match δ with the uncertain loading d.

The next section will explore further conditions on the RIO parameters to guarantee stability of the human-intended oscillation z_d as a solution to the closed-loop system.

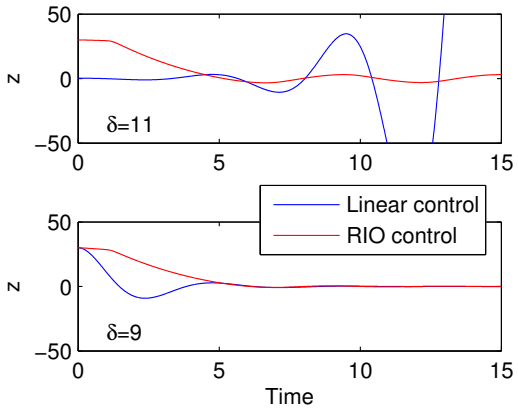

Fig. 2: Mechanical-RIO system behavior without human input

C. Stability of the Periodic Solution

Consider the closed-loop system consisting of the plant (1), human control (6), and the RIO control (7). We assume that the human control is chosen as in (6) to make the target oscillation z_d in (2) a solution of the closed-loop system. In Theorem 1, a condition for the RIO to compensate for damping in the steady state is provided. This section will analyze the transient response and provide additional conditions under which convergence to the target oscillation z_d is theoretically guaranteed. After a formal statement of the stability condition, we will discuss robustness against uncertainties in the human motor control parameters (α, β) and develop a design procedure that does not depend on the knowledge of (α, β).

First note that the closed-loop system can be expressed as

$$\begin{aligned} \ddot{z} &= G\Psi(\dot{p})/m + \gamma/m - d_\alpha \dot{z} - k_\beta z \\ \ddot{p} &= 2\varpi(L\Psi(\dot{p}) + Hz - \dot{p}) - \varpi^2 p \end{aligned} \tag{13}$$

where $p \in \mathbb{R}^2$ is a state associate with the transfer function $b(s)$ and is related to q by $\dot{p} = q$, and

$$\begin{aligned} &k_\beta := (k-\beta)/m, \quad d_\alpha := (d-\alpha)/m, \\ &\gamma := v_d - \alpha \dot{z}_d - \beta z_d. \end{aligned}$$

It can be verified that $(z, p) = (z_d, p_d)$ is a solution of (13) where p_d is a periodic signal such that $\dot{p}_d = x_d l$ and the average of p_d over a cycle is zero, with x_d being a periodic solution to (10). The linearization of (13) around $(z, p) = (z_d, p_d)$ is given by the linear T-periodic system

$$\dot{\eta} = A(t)\eta \tag{14}$$

where $T := 2\pi/\omega_d$ and[3]

$$\eta := \mathrm{col}(z_e, \dot{z}_e, p_e, \dot{p}_e), \quad z_e := z - z_d, \quad p_e := p - p_d,$$

$$A = \begin{bmatrix} 0 & 1 & 0 & 0 \\ -k_\beta & -d_\alpha & 0 & (g/m)\psi'(x_d)l^\intercal \\ 0 & 0 & 0 & I \\ 2\varpi h l & 0 & -\varpi^2 I & 2\varpi(\psi'(x_d)L - I) \end{bmatrix}. \tag{15}$$

As is well known [31], exponential stability of the trajectory (z_d, p_d) for the original nonlinear system (13) is equivalent to exponential stability of the linearized system (14). According to a result in [33] (Theorem 2 on page 36), the linear periodic system (14) is asymptotically stable if $\bar{A}$ is Hurwitz and $\|\mathscr{E}\|_\infty$ is sufficiently small, where

$$\bar{A} := \frac{1}{T}\int_0^T A(t)dt, \quad \mathscr{E}(t) := A(t) - \bar{A},$$

and $\|\mathscr{E}\|_\infty$ is the maximum of $\|\mathscr{E}(t)\|$ over a cycle. Based on this stability condition, we reach the following result.

Theorem 2: Consider the closed-loop system consisting of the plant (1)*, human control* (6)*, and RIO control* (7)*. Suppose the human chooses* (α, β) *such that*

$$k_\beta := \frac{k-\beta}{m} > 0, \quad d_\alpha := \frac{d-\alpha}{m} > 0. \tag{16}$$

Then $z_d(t)$ *in (2) is a solution of the closed-loop system. Let positive scalars* $\delta, \varpi \in \mathbb{R}$ *be given such that*

$$0 < \frac{\omega_d^2 - \varpi^2}{\omega_n^2 - \varpi^2} < r := \frac{d-\alpha}{\delta}, \quad \omega_n := \sqrt{k_\beta} \tag{17}$$

Then, for each $\mu > 1$ *with sufficiently small* $\mu - 1$*, there exists an* h *with sufficiently small* $|h|$ *such that a* T*-periodic solution* x_d *to (10) exists and* $z_d(t)$ *is a stable solution of the closed-loop system, where the remaining RIO parameter* g *is chosen to satisfy (11a).*

If the human control parameters (α, β) and the intended oscillation $z_d(t)$ were precisely known in advance and satisfied (16), then Theorem 2 and its proof suggest the following design procedure for the RIO control. First, choose positive scalars $\delta, \varpi \in \mathbb{R}$ satisfying (17). Grid the ζ parameter space and numerically calculate the roots λ_i of the characteristic equation $\det(\lambda I - \bar{A}) = 0$ to plot the largest real part $\max \Re[\lambda_i]$ as a function of ζ. Theorem 2 guarantees that the value at $\zeta = 0$ is negative, and hence by continuity there exists $\varepsilon > 0$ such that $\max \Re[\lambda_i] < 0$ for all $|\zeta| < \varepsilon$. Fix $\mu \in \mathbb{R}$ within the interval $1 < \mu < 1 + \varepsilon$. Grid the h parameter space and numerically calculate the maximum Floquet multiplier τ of the linearized system as a function of h, where

$$\tau(h) := \max |\mathrm{eig}(\Phi(T))|, \quad \dot{\Phi} = A\Phi, \quad \Phi(0) = I.$$

Theorem 2 guarantees that $|\tau(h)| < 1$ and the linearized system is stable when $|h|$ is sufficiently small. Choose a value of such h. The resulting RIO control stabilizes $z_d(t)$.

In reality, the human control parameters (α, β) are uncertain, and the intended oscillation $z_d(t)$ may not be decided in advance or may vary over time. Thus, the design procedure described above does not apply exactly. However, the RIO control may be designed to maintain stability of $z_d(t)$ robustly against uncertainties in (α, β) and $z_d(t)$. In particular, Fig. 3 shows the region on the (ϖ, r) plane in which the stability condition (17) is satisfied. We see that the stability is maintained in a large region in the parameter space, and hence the design is robust against perturbations in the human motor control parameters. Thus, fine tuning of the design parameters, based on precise values of the human parameters, is unnecessary.

Moreover, the result provides a qualitatively robust guideline for the control design that can be used for model-free, on-site parameter tuning. In particular, from Theorem 2, stability of the target oscillation is theoretically guaranteed, *regardless*

[3]Here, $\mathrm{col}(x_1, \ldots x_n)$ denotes the column vector with entries $x_1, \ldots, x_n$.

of the human parameters, if the intrinsic frequency ϖ of the RIO is chosen sufficiently large or small, and if the amount of damping compensation δ is sufficiently small (i.e., r is large). Hence, with a fixed ϖ, the value of δ can be gradually increased at the experimental site until the human force becomes the smallest. This is the design procedure we used and validated in our experiments reported later. It should be noted that the design process is model free, and does not require identification of the model (6) for the human motor control.

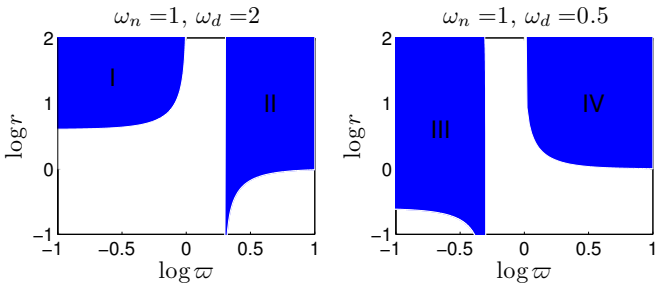

Fig. 3: Stability regions (shaded) for (ϖ, r) satisfying (17). Case $\omega_n < \omega_d$ (left) and Case $\omega_d < \omega_n$ (right). The vertical asymptotes are at $\varpi = \omega_n$ and ω_d, while the horizontal asymptotes are at $r = 1$ and $(\omega_d/\omega_n)^2$.

III. Experimental Validation

A. Assistive Control Test Rig

We built a one-link robotic arm to test and validate the assistive CPG control method proposed in the previous section. The experimental test rig is shown in Fig. 4. The system emulates a situation where a human and a robot grab a common tool to stir viscous fluids. The robotic arm of length 0.3 m and mass 2.0 kg is driven by a servo motor with a gear box (Harmonic Drive FHA-17C-100, gear ratio 1:100) to rotate around its shoulder joint within a horizontal plane. The rotational angle of the motor is measured by an encoder. A force sensor (Futek MBA400) is fixed at the end-tip of the robotic arm with a handle attached to it. A human grabs the handle and applies torque through the handle, while the measured force and angular position data are collected by the sensors and fed back to the control computer. The computer (Speedgoat performance real-time target machine) generates an appropriate control command signal to the servo motor and records the sensor measurements.

The intended operation of the system can be explained using the diagram shown in Fig. 5. A human grabs the handle at the end of the robotic arm. The arm angle is visually shown on the computer screen as a blue circle. A reference position of the arm is also shown on the screen as a red star. While the red star goes back and forth to indicate sinusoidal oscillation of the reference arm angle z_d, the human is asked to apply force so that the actual arm angle z follows the reference position (i.e. the blue circle tracks the red star). The force sensor measurement will then indicate the human effort required for the periodic operation.

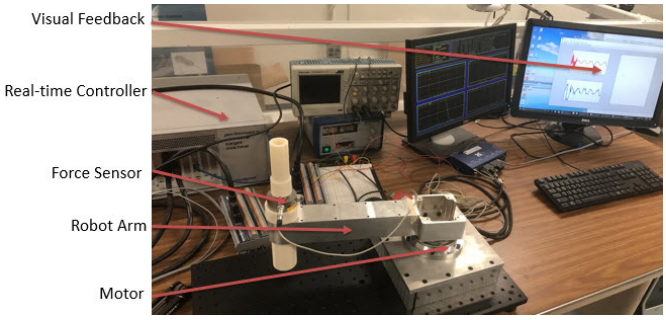

Fig. 4: Experimental test rig (hardware)

This experiment is repeated with and without an assistive CPG-based controller. The controller is designed to drive the arm through the servo motor so that the human effort is reduced while achieving the same or better tracking performance. The CPG controller uses only the encoder measurement of the robot arm angle as sensory feedback. The controller is deemed effective if the human effort is smaller with the controller than without it, while achieving the same or better tracking performance. The experiments are conducted under two loading conditions: a virtual load that electronically emulates a mass-damper system, and a physical load to stir high viscosity fluid by an effector attached at the arm end.

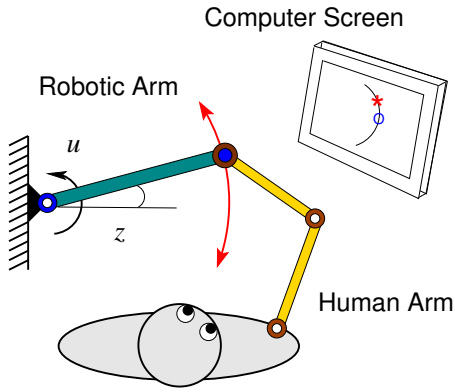

Fig. 5: Schematic of human-robot experiment

B. Modeling of Human Motor Control

The assistive CPG control design does not require a model for the human motor control. However, the design theory guarantees stability of the periodic trajectory when the human control can be modeled as in (6) and satisfies (16). Hence we perform system identification of the human motor control to validate our theory.

1) Framework and approach: When a human moves an object along a desired periodic trajectory, s/he would use a certain control strategy to achieve the movement. For the single-DOF mechanical system described by (1) with $u(t) = 0$, the human motor control may be modeled by

$$v(t) = \hat{m}\ddot{z}_d + \hat{d}\dot{z}_d + \hat{k}z_d + \alpha(\dot{z} - \dot{z}_d) + \beta(z - z_d), \quad (18)$$

where $z_d(t)$ is the desired trajectory, $(\hat{m}, \hat{d}, \hat{k})$ are the mass, damping, and stiffness parameters assumed by the human,

and (α, β) are the feedback gains to generate corrective forces/torques. This mathematical model is consistent with the literature on human motor control, where the human is often found to employ both feedforward and feedback strategies. The feedforward action is captured by the term of the control model $\hat{m}\ddot{z}_d + \hat{d}\dot{z}_d + \hat{k}z_d$, which is the human estimated force appropriate for achieving the motion $z_d(t)$ and can be refined through experience. The feedback action is captured by the term $\alpha(\dot{z}_d - \dot{z}) + \beta(z_d - z)$, which adjusts the applied force in accordance with the error between the desired and actual trajectories. The feedforward/feedback model in (18) was assumed for the human motor control when we developed the assistive CPG control theory. The objective here is to identify the parameters $(\hat{m}, \hat{d}, \hat{k})$ and (α, β) and validate the human motor control model (18) and stability condition (16).

During the experiments, the dynamics from human torque input v to the arm angular velocity $\dot{z}$ are set via a minor feedback loop for the servo motor to match the reference model $M(s) := s/(ms^2 + ds + k)$ for a single-DOF mass-damping-stiffness system. In the transfer function, m, d, k are virtual system mass, damping and stiffness parameters, assigned by the software. The velocity command r is calculated as the output of the virtual system $M(s)$ when the input v is applied. The motor velocity is regulated by a high-gain PID controller $K(s)$ to track the reference command r.

The system block diagram is shown in Fig. 6, where G represents the physical dynamics of the arm-gear-motor system from the torque input to the angular velocity output, $K(s)$ is the PID controller within the servo unit under the velocity mode, and Q represents the electromagnetic dynamics from the PID output to the actual torque τ generated by the motor. Ideally, the velocity $\dot{z}$ matches the command so that the overall dynamics from v to $\dot{z}$ have the desired mechanical impedance $(ms + d + k/s)$. From Fig. 6, we see that the arm-gear-motor system G receives both τ and v as inputs, and this v could act as a disturbance for the PID control system. However, it was verified during the experiments that the high gain control $K(s)$ made the velocity $\dot{z}(t)$ almost overlap with the reference $r(t)$ when plotted, and thus achieved the desired mechanical impedance.

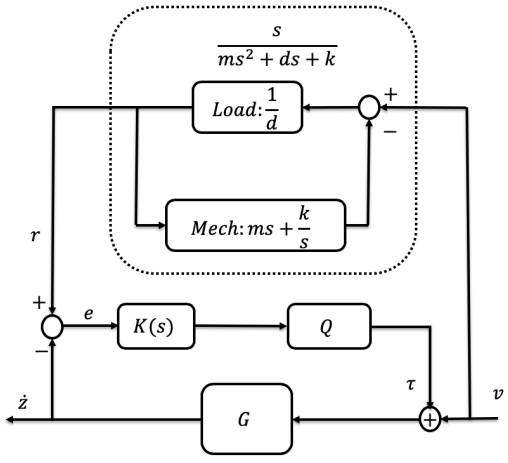

Fig. 6: Virtual impedance set by minor feedback

While the human tracks a desired trajectory by moving the arm as described earlier, the time histories of the variables $z(t)$, $z_d(t)$, and $v(t)$ are recorded at time instants $t = t_i$ for $i = 1, \ldots, n$ where n is the number of data points collected. The data is fit by the human motor control model (18) through the least square optimization:

$$\min_x \|b - Ax\| \tag{19}$$

where

$$\begin{aligned} &x = \text{col}(\hat{m}, \hat{d}, \hat{k}, \alpha, \beta), \\ &b = \text{col}(v(t_1), v(t_2), ..., v(t_n)), \\ &A = \text{col}(a(t_1), a(t_2), ..., a(t_n)), \\ &a(t) = \begin{bmatrix} \ddot{z}_d(t) & \dot{z}_d(t) & z_d(t) & \dot{z}(t) - \dot{z}_d(t) & z(t) - z_d(t) \end{bmatrix}. \end{aligned}$$

To assess the importance of the feedforward and feedback terms, we also consider the feedforward controller

$$v_{ff} = \hat{m}\ddot{z}_d + \hat{d}\dot{z}_d + \hat{k}z_d, \tag{20}$$

and feedback controller

$$v_{fb} = \alpha(\dot{z} - \dot{z}_d) + \beta(z - z_d). \tag{21}$$

The corresponding optimization problems can be formulated as (19) with

$$x = \text{col}(\hat{m}, \hat{d}, \hat{k}), \quad a(t) = \begin{bmatrix} \ddot{z}_d(t) & \dot{z}_d(t) & z_d(t) \end{bmatrix}.$$

for the feedforward model and

$$x = \text{col}(\alpha, \beta), \quad a(t) = \begin{bmatrix} \dot{z}(t) - \dot{z}_d(t) & z(t) - z_d(t) \end{bmatrix}.$$

for the feedback model.

The accuracy of the mixed feedforward/feedback model (18) is evaluated by applying it as the controller to the system and comparing the resulting motion with the recorded motion under the human control. In particular, for a fixed reference position $z_d(t)$, the human or the model (18) drives the system to track it, and the resulting motion is denoted as $z(t)$ or $z_m(t)$, respectively. The human input $v(t)$ adds to $\tau(t)$ as in Fig. 6, but the model input $v(t)$ does not add to τ since no physical force is applied directly to the arm. The difference is considered negligible since $\tau \gg v$ due to the high gear ratio. The correlation between z and z_m is calculated as follows:

$$r_m = \frac{\sum_{k=1}^n z(t_k) z_m(t_k)}{\sqrt{(\sum_{k=1}^n z^2(t_k))(\sum_{k=1}^n z_m^2(t_k))}}.$$

The correlation r_m will be 1 if z_m matches z perfectly, and hence closeness of r_m to 1 indicates accuracy of the human control model (18). Similarly, feedforward controller (20) and feedback controller (21) are evaluated by the correlations r_{ff} and r_{fb}, where z_{ff} and z_{fb} are the measured angles during the experiments in which the system is driven by $z_d(t)$ under the control (20) and (21), respectively.

2) Experimental result and discussion: During the experiment, we assigned different values to m and d virtually in the software using minor feedback control (velocity servo mode), while the stiffness was set to $k = 0$. The desired oscillation is

$$z_d(t) = \frac{\pi}{3} \sin(\frac{2\pi}{9} t). \tag{22}$$

For each m and d values, the experiment was conducted for 15 times and 50 seconds for each run. The measurements of the force sensor and encoder were collected as frequently as possible within the hardware limitation, so the sampling period $(t_{i+1}-t_i)$ was not fixed constant. However, this does not affect the formulation of the optimization problems that identify the model parameters.

The result of the parameter identification for the three human control models, (18), (20) and (21), are shown in Table I, where $\hat{k}$ was set to zero during the optimization. For the mixed model (18), the feedforward parameters $(\hat{m}, \hat{d})$ are very close to the actual mass and damping values (m, d), the rate feedback gain α is slightly less than the damping d to mostly compensate for the damping load while maintaining stability, and the position feedback gain β is negative so that stiffness is added for achieving the oscillation task. The closed-loop system is given by

$$m\ddot{z} + (d-\alpha)\dot{z} - \beta z = \hat{m}\ddot{z}_d + (\hat{d}-\alpha)\dot{z}_d - \beta z_d.$$

It is observed that the human chooses the control parameters so that the dynamics on the left hand side have the natural frequency around $\omega_n = 1 \sim 1.5$ rad/s (e.g. $1.14 \sim 1.25$ for $m = 5$), which is slightly larger than but in the same order as the driving frequency $\omega_d = 2\pi/9 = 0.7$ of the reference signal $z_d(t)$. Moreover, the human-compensated damping $d - \alpha$ and stiffness $k - \beta$ are always positive, and assumption (16) is satisfied.

Another set of experiments were conducted to validate the obtained human control models. In particular, for each system parameter value of (m, d), the following four experiments were conducted with the common $z_d(t)$ in (22), where $u = 0$ in system (1):

- A human applies v to system (1).
- The mixed model controller (18) applies v to system (1).
- The feedforward controller (20) applies v to system (1).
- The feedback controller (21) applies v to system (1).

In the first experiment, force v is directly applied by a human through the handle. In the other experiments, v is generated by the motor mounted on the robotic arm. Then during each experiment, $z(t)$, $z_d(t)$, and $v(t)$ are measured and the data of $z(t)$ are used to compute the correlations r_m, r_{ff}, and r_{fb}. The results of the correlation analysis are summarized in Tables II and III. In the tables, $*$ indicates that the controller failed to stabilize the system and the resulting correlations were negative. For the results in Table II, the initial condition was set to $z(0) = \dot{z}(0) = 0$ which matches with the initial value of the desired oscillation $z_d(0) = \dot{z}_d(0) = 0$, while for Table III, the initial condition was $z(0) = \pi/4$ and $\dot{z}(0) = 0$, which is away from the initial value of the desired oscillation $z_d(t)$.

In general, the mixed human motor control model (18) shows good correlation. In cases where the initial state is aligned with the desired trajectory z_d (Table II), the feedforward control model (20) achieves high correlations. However, in cases where the initial state differs from the desired trajectory (Table III), the feedforward control model (20) exhibits lower correlations than those of the mixed control model (18).

TABLE I: Human Control Model Parameter

m = 2					
	d	5	10	15	18
Mixed Model	$\hat{m}$	2.01	2.38	2.33	2.49
	$\hat{d}$	4.95	10.10	14.93	17.86
	α	4.72	8.52	14.72	17.89
	β	−4.02	−1.02	−4.84	−3.87
Feedforward	$\hat{m}$	1.98	1.60	1.69	1.19
	$\hat{d}$	5.08	9.79	15.31	18.16
Feedback	α	5.39	5.04	17.77	18.26
	β	−6.70	−1.46	−15.64	−25.46
m = 5					
	d	5	10	15	18
Mixed Model	$\hat{m}$	5.05	5.51	5.37	5.46
	$\hat{d}$	4.62	10.13	14.85	18.00
	α	3.95	7.20	14.19	16.69
	β	−7.81	−7.58	−7.21	−6.54
Feedforward	$\hat{m}$	4.81	5.01	4.28	4.15
	$\hat{d}$	5.19	10.44	15.44	18.57
Feedback	α	1.64	4.22	13.58	16.71
	β	−15.16	−17.82	−26.08	.25.23

TABLE II: Model Validation: $z(0) = z_d(0)$

	m = 2			
d	5	10	15	18
r_m	0.841	0.946	0.807	0.633
r_{ff}	0.947	0.966	0.969	0.974
r_{fb}	$*$	−0.832	$*$	$*$
	m = 5			
d	5	10	15	18
r_m	0.950	0.973	0.915	0.901
r_{ff}	0.741	0.868	0.972	0.938
r_{fb}	0.948	0.929	0.599	0.847

TABLE III: Model Validation: $z(0) \neq z_d(0)$

	m = 2			
d	5	10	15	18
r_m	0.848	0.950	0.889	0.937
r_{ff}	0.845	0.720	0.707	0.685
r_{fb}	0.638	−0.785	0.426	0.450
	m = 5			
d	5	10	15	18
r_m	0.929	0.989	0.938	0.945
r_{ff}	0.970	0.866	0.765	0.749
r_{fb}	0.958	0.915	0.826	0.830

Regardless of the initial conditions, the feedback control model gives the worst performance. Thus, feedforward action seems essential in the human motor control, while feedback action would also be included for corrective behavior.

C. Assistive Control

1) Problem formulation and approach: We design an assistive CPG controller for the robotic arm and experimentally validate its performance. The controller should drive the robotic arm to provide assistance when human tries to maintain a rhythmic movement of the robotic arm. That is, the CPG control is considered to be effective if the human is able to maintain a similar oscillation with less effort than required without the additional robotic system.

The robotic arm system can be approximately described by (1) where $v(t)$ is the toque applied by the human and $u(t)$ is the toque applied by the assistive controller.

A human subject is asked to perform the same task as described in Section III-A, under various loading conditions with and without the assistive control. The human-applied torques were recorded and compared to evaluate the effort reduction. The actual trajectory of the end-tip was compared with the desired trajectory to evaluate the performance of the human control. A human would be able to achieve good tracking for a plant with passive dynamics (i.e. without the assistive control), and a similar performance is expected if the assistive CPG control does not add dynamics that are felt as unnatural by the human. Theoretically, our controller is guaranteed to achieve stability of the targeted trajectory, provided the human motor control is of the form (18) with $d > \alpha$ and $k > \beta$. We expect that the stability property makes the human feel easy to control the plant.

2) Virtual load experiments: As in the case of the human control modeling, the virtual mechanical impedance (m, d, k) is specified through the minor feedback in the velocity mode as described in Section III-B1. In this virtual experiment, we attribute the mass and stiffness effect to a robotic system and the damping effect to a load. With the RIO control, the system in Fig. 6 has an additional outer loop that goes from z (generated by multiplying $1/s$ to $\dot{z}$) through the RIO to its output u which is added to v before entering the reference model block $M(s)$. The block diagram is shown in Fig. 7, where the block labeled by "RIO" denotes the nonlinear mapping from z to u defined by (7).

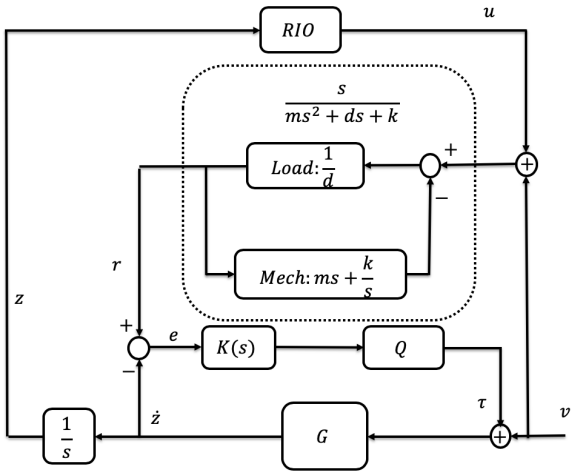

Fig. 7: Virtual load system with RIO control

We fixed $k = 0$ and varied system parameters m and d to test the assistive effect of the RIO control. The desired oscillation was set as in (22). The RIO controller parameters were designed based on the steps in Section II-C. The desired damping compensation was set to be $\delta = 10$ and other parameters were selected as

$$h = 0.1, \quad \mu = 1.001, \quad \varpi = 10, \quad g = 225.$$

The intrinsic frequency ϖ of the RIO is chosen to be much larger than the expected operating frequency range (roughly 1 rad/s) in accordance with Fig. 3. Based on the modeling result for human motor control in the previous section, we expect that the human chooses stiffness β so that the natural frequency ω_n is slightly larger than the operating frequency ω_d. In this case, the value of r larger than roughly 1 would result in stability as indicated in Fig. 3 (right). In the best scenario, d is slightly larger than $\delta = 10$ so that the RIO compensates for most of the damping and the human achieves the desired oscillation using small effort ($\alpha = 0$) with stability (17). The control performance is tested under various loading conditions where the value of d can be away from 10 and the linear model $d\dot{z}$ may contain large errors.

The experimental result is shown in Fig. 8. The average error defined as

$$\text{average error} = \frac{\sum_{k=1}^{n} |z(t_k) - z_d(t_k)|^2}{\sum_{k=1}^{n} |z_d(t_k)|^2}$$

indicates the amount of errors in tracking the reference trajectory $z_d(t)$. When RIO is on, the average effort defined as

$$\text{average effort} = \frac{\sum_{k=1}^{n} |v(t_k)|^2}{n}$$

indicates the amount of human effort in achieving the trajectory tracking. When RIO is off, the average effort is defined as the amount of force squared for virtual damping compensation

$$\text{average effort} = \frac{1}{T} \int_0^T |d\dot{z}_d(t)|^2 dt,$$

which is the human effort without assistance by a robotic device.

Each dot represents one episode of experiment with running time 60 seconds. The actual collected data points are not evenly distributed in time and thus interpolated into a new sequence with equal time step $t_{k+1} - t_k = 0.1$ second. In this process, the data points during the first and last 1 second are omitted because of the interpolation. Therefore, the number of the resulting sampling points, n, is slightly less than 600.

The average effort is clearly smaller with the RIO control than without it for all the cases shown in Fig. 8. The effort reduction is larger when the damping load is larger, but is roughly the same for $m = 2$ and 5 under the same damping load. This is exactly what is expected since the RIO control is designed to compensate for the damping effect. We see that the average error for tracking is larger with heavier mass, but is consistently smaller with the RIO control than without it when $d > \delta = 10$. This result agrees with our expectation since, in those cases, the stability condition (17) would be met with $\alpha \cong 0$, making it easier for the human to track the desired oscillation.

3) Physical load experiments: In the previous section, the mechanical impedance of the plant was set by minor feedback with high gain PID control, using the electrical signal of human torque measurement as the input to the system. Here, we consider combining the virtual mechanical impedance with a physical load to test robustness of the RIO control against complex loading dynamics that are difficult to emulate.

For this experiment, a cylindrical end effector is attached to the end-tip of the robotic arm and is submerged into a mixed viscous fluid, which serves as the physical load of the system. A picture of the system is shown in Fig. 9. The fluid is made

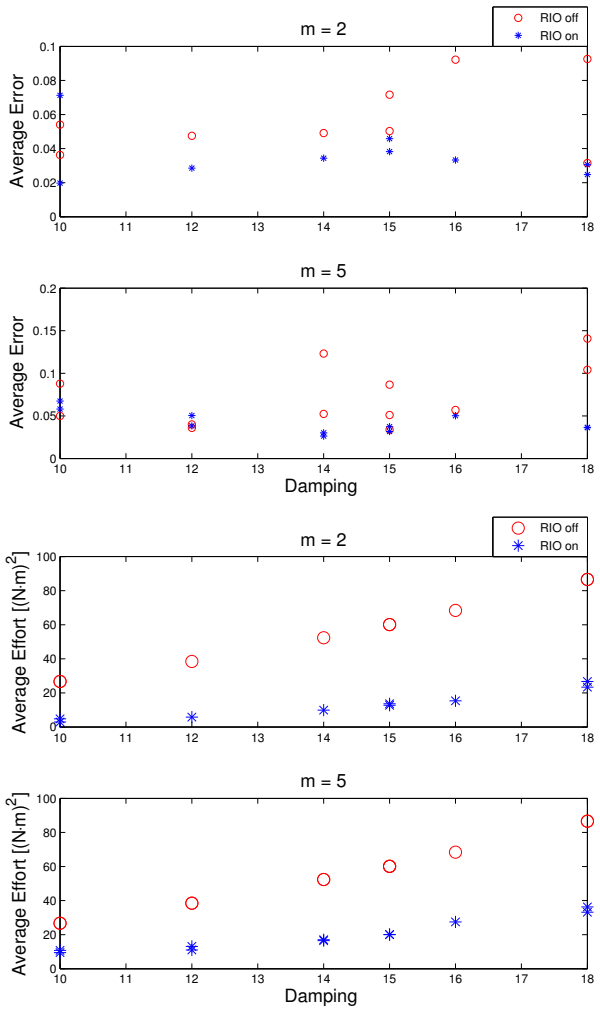

Fig. 8: Comparisons of human effort and tracking error

by adding food thickeners to water, increasing the viscosity and density. Since the intended arm motion is rather slow (e.g. oscillation period 4 s with peak-to-peak amplitude 23 cm), the resistive hydrodynamic force is expected to dominate over the reactive force or the added mass effect.

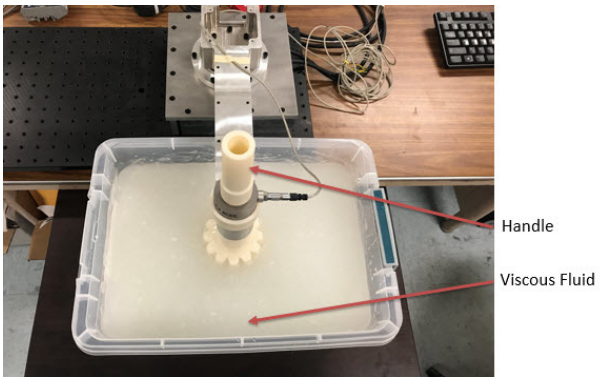

Fig. 9: Physical Load

When the physical load is attached to the robotic arm, the system is described by the diagram in Fig. 10, where G represents the arm-gear-motor mechanical dynamics, D represents the viscous fluid load, and the block labeled as "RIO" is the nonlinear mapping of the RIO controller in (7) from z to u. We set up the system so that physical human toque v directly acts on the robotic arm, and the human force measurement is used only for monitoring the human effort (not for affecting the servo motor torque). The torque control mode is used for the servo motor, where the output torque τ is (approximately) proportional to the command signal w. The electromagnetic dynamics from w to τ are represented by E in the figure, and is modeled by $E_m(s)$. The control command signal is set by the RIO controller, through the inverse dynamics $E_m(s)^{-1}$ that approximately cancels E so that $\tau \cong u$. Based on the design guideline described earlier, the RIO controller parameters were chosen as

$$\delta = 25, \quad h = 0.1, \quad \mu = 1.001, \quad \varpi = 10, \quad g = 562.$$

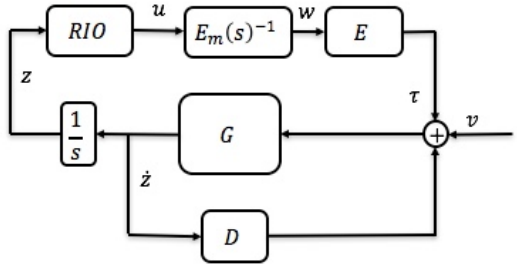

Fig. 10: Robotic arm G with physical damping D, driven by human torque v and RIO control u

While the control design is essentially model free, the theoretical analysis of stability and performance is based on the simple plant model in (1). The actual plant comprises the physical dynamics of the arm-gear-motor G, fluid load D, and actuation dynamics E. To provide a physical sense of the plant, these components are very roughly modeled as (see Appendix C)

$$\begin{aligned} G_m(s) &= 1/(1.12s + 22.5), \quad E_m(s) = 3.13, \\ D_m(s) &= -(0.056s + 3.33), \end{aligned} \tag{23}$$

indicating that the physical plant is modeled by (1) with effective moment of inertia $m = 1.18$ kg·m^2, damping $d = 25.8$ Nms, and stiffness $k = 0$. The model is very crude, missing higher order dynamics and nonlinear effects. Our goal is to demonstrate that the RIO control is effective in the presence of such unmodeled dynamics and nonlinearities.

During the experiment, the human grabs the handle and tries to rotate the robotic arm, with/without the help from the RIO controller, to track a desired oscillation given by

$$z_d(t) = \frac{\pi}{8} \sin\left(\frac{\pi}{2} t\right),$$

while the hydrodynamic resistive force is measured by a force sensor mounted between the cylindrical end effector and the arm. At this frequency, the damping effect dominates the load; the amplitude of the inertia torque is roughly $m\omega_d^2 a_d = 1.1$ Nm while that of the damping torque is $d\omega_d a_d = 15.9$ Nm, and that of the fluid load is around 8 Nm. The RIO control

is supposed to reduce the load by $\delta\omega_d a_d = 15.5$ Nm. The experimental measurements are shown in Fig. 11. It can be seen that when the RIO control is turned on at $t = 40$ s, the human effort is reduced as expected, while the human subject maintains good tracking of the reference trajectory. The remaining human force with RIO assistance has an amplitude about 3 Nm, where roughly 62% reduction is achieved when compared with the hydrodynamic damping load itself.

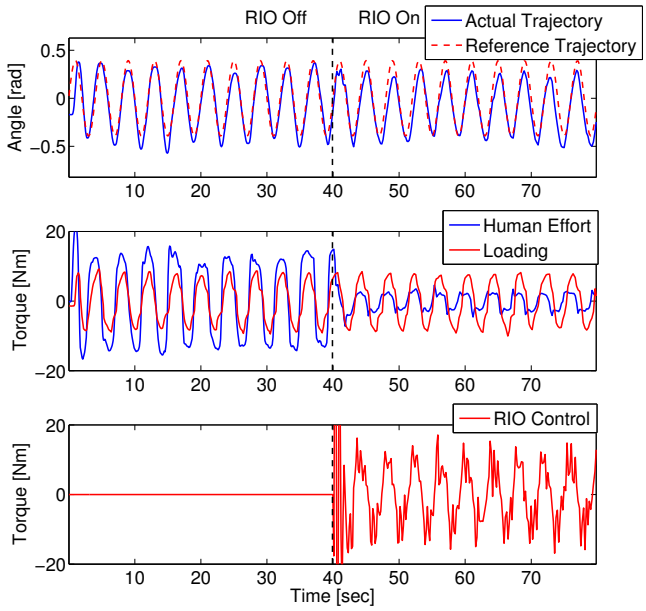

Fig. 11: Effect of RIO control on human effort reduction

Since the RIO control essentially compensates for the damping effect, the human force under RIO assistance will be roughly equal to the force required for driving the inertia/stiffness dynamics of the assistive robotic system. Hence, the human effort reduction is expected when the load resistance force is larger than the robotic inertia/stiffness force, and the effectiveness of the RIO control depends on how much difference exists between these two forces.

IV. Conclusion

We have considered the situation where a human and a feedback controller cooperate to drive a single-DOF mechanical system in order to achieve a human-intended oscillation. A control design method is proposed, based on the reciprocal inhibition architecture of the CPG, such that the human-intended oscillation is stabilized while the human effort is reduced by a nonlinear damping compensation. Analytical formulas are derived for the control design parameters, and local stability of the target trajectory is rigorously proven, assuming a mixed feedforward-feedback structure of the human motor control. The design is essentially model-free, and the parameters can be chosen without detailed knowledge of the mechanical and human dynamics, thus achieving robustness against uncertainties.

We proposed a model structure for human motor control that combines feedforward and feedback actions. The model is of independent interest for understanding how a human controls his/her motion, and for developing devices that interact with humans. The model parameters were identified using experimental measurements of human generated toque, robotic arm position (angle), and its reference command. The model was validated by a separate set of experimental data, obtained under multiple initial conditions. It was found that the feedforward action is important for human motor control, but the feedback action is also used to cancel the damping effect and set the natural frequency slightly above the operating frequency. The identified model parameter values confirmed that the RIO controller can be designed to satisfy the stability condition.

An RIO assistive controller was designed using the theoretical result, and the assistive performance of the control system was tested experimentally. A test rig of a single-DOF robotic arm was built with a servo motor, an encoder, and a force sensor, for testing under two conditions - virtual load with various mechanical impedance values set by a minor feedback, and physical load of viscous fluid with uncertain and complex dynamics. The arm-gear-motor system with virtual/physical loads were driven by the RIO controller and human force inputs. Numerous experiments were conducted to verify that, under both loading conditions, the RIO control was capable of reducing the human effort without degrading the tracking performance of the human to follow an oscillatory reference movement.

Although the theoretical result on stability is proven for sinusoidal target motion, we expect that our control design would be effective in reducing the human burden to some extent, also for non-sinusoidal periodic motions close to sinusoids. The rationale for this expectation is that the RIO acts as a nonlinear damping compensator for the fundamental harmonic component of such motions. This expectation was met in our experiments where the angular oscillation was non-sinusoidal as in Fig. 11.

Finally, we remark on some possible extensions. One direction is exploitation of force sensors. While the proposed RIO control compensates for the damping effect, we expect that it would be possible, with additional force feedback, to compensate also for the inertia effect. However, it is not clear how such force feedback can be effectively utilized in the CPG framework within the assistive control context. Another direction is optimization of the controller parameters. The proposed method allows for on-site tuning of the RIO parameter δ for maximal reduction of the human effort in the steady state. It would also be of practical importance to optimize other RIO parameters for reduction of the *transient* human burden to stabilize the target oscillation. Our result addressed the minimal qualitative requirement of stability, and may provide a foundation for further quantitative analysis and optimization of the transient performance.

Appendix

A. Technical results

Lemma 1: Consider the linear system

$$\dot{x} = Ax + Bu, \quad y = Cx,$$

which may or may not be stable. Let $T > 0$ be given and suppose A has no eigenvalue at $\pm j\omega k$ for any integer k, where $\omega := 2\pi/T$. Then, for an arbitrary T-periodic input $u(t)$, there exists an initial state $x(0)$ that yields T-periodic state $x(t)$ and output $y(t)$. In particular, the T-periodic solution is uniquely given by

$$y(t) = \int_0^T H(\tau)u(\tau + t)d\tau,$$
$$H(\tau) := C(I - e^{AT})^{-1}e^{A(T-\tau)}B$$

Moreover, the peak values of the input and output are related by

$$||y||_\infty \le c||u||_\infty, \quad c := \int_0^T ||H(t)||dt.$$

Proof: The general solution is given by

$$x(t) = e^{At}x(0) + \int_0^t e^{A(t-\tau)}Bu(\tau)d\tau.$$

The solution is T-periodic, $x(t) = x(t+T)$, when

$$x(0) = e^{AT}x(0) + \int_0^T e^{A(T-\tau)}Bu(\tau)d\tau,$$

which can be solved for

$$x(0) = (I - e^{AT})^{-1}\int_0^T e^{A(t-\tau)}Bu(\tau)d\tau,$$

where we note that e^{AT} has eigenvalues at $e^{\lambda T}$ with λ being an eigenvalue of A, and hence $I - e^{AT}$ is invertible due to the supposition. Substituting the initial state into the general formula, we have

$$\begin{aligned} x(t) &= e^{At}(I - e^{AT})^{-1}\int_0^T e^{A(T-\tau)}Bu(\tau)d\tau \\ &\quad + \int_0^t e^{A(t-\tau)}Bu(\tau)d\tau \\ &= (I - e^{AT})^{-1}\int_0^T e^{A(T-\sigma)}Bu(\sigma + t - T)d\tau \end{aligned}$$

The formula for $y(t)$ directly follows from this equation. The bound on the peak-to-peak gain can be seen from

$$\begin{aligned} ||y(t)|| &= ||\int_0^T H(\tau)u(\tau + t)d\tau|| \\ &\le \int_0^T ||H(\tau)|| \cdot ||u(\tau + t)||d\tau \\ &\le \int_0^T ||H(\tau)|| \cdot ||u||_\infty d\tau = c||u||_\infty. \end{aligned}$$

■

Lemma 2: Consider the harmonically forced nonlinear system

$$x = b(s)(\mu\psi(x) + hz), \quad z(t) = a\sin(\omega t) \tag{24}$$

where $x(t) \in \mathbb{R}$ is a scalar variable, $b(s)$ is a strictly proper transfer function, $\mu, h, a, \omega \in \mathbb{R}$ are nonzero constants, and $\psi(x) := \tanh(x)$. Suppose $\omega > 0$ and

$$b_\mu(s) := \frac{b(s)}{1 - \mu b(s)}$$

has no poles on the imaginary axis. Then, for sufficiently small $|h|$, there exists a T-periodic solution $x(t)$ in the neighborhood of the origin, where $T := 2\pi/\omega$. Let such solution be denoted by $x_h(t)$ for each h. There exists a constant γ such that

$$\|x_h\|_\infty \le \gamma|h|.$$

Moreover, we have

$$\lim_{h\to 0}\frac{1}{h}\Big(\psi'(x_h(t)) - \kappa(x_h(t))\Big) = 0, \quad \forall t \in \mathbb{R}.$$

Proof: We assume that h is positive without loss of generality since the sign of h can be absorbed into a. All the trajectories of the forced nonlinear system with various values of h can be captured by the autonomous nonlinear system

$$x = b(s)(\mu\psi(x) + \xi), \quad \ddot{\xi} + \omega^2\xi = 0. \tag{25}$$

The linearization of the system (25) around the origin is given by

$$x = b_\mu(s)\xi, \quad \ddot{\xi} + \omega^2\xi = 0. \tag{26}$$

By Lemma 1, the linearized system has a harmonic solution $x(t)$ in the neighborhood of the origin with $\xi(t) = hz(t)$ for sufficiently small h, where its peak value approaches zero as h goes to zero. By a version of the Grobman-Hartman result [34], there exists a (time-preserving) homeomorphism between trajectories in the neighborhoods of the origins of the two systems (25) and (26). Therefore, we infer that the original nonlinear system (24) has a T-periodic solution $x_h(t)$ for sufficiently small h, where its peak value α_h approaches zero as h goes to zero.

Now, let $y_h(t) := x_h(t)/\alpha_h$ and note that the system dynamics (24) imply

$$\begin{aligned} y_h = b_\mu(s)v_h, \quad & v_h := \mu\phi_h(y_h) + (h/\alpha_h)z, \\ & \phi_h(x) := \psi(\alpha_h x)/\alpha_h - x \end{aligned}$$

Then, by Lemma 1, there exists $c > 0$, independent of h, such that $||y_h||_\infty \le c||v_h||_\infty$. Since $||y_h||_\infty = 1$ by definition, we have $1 \le c||v_h||_\infty$ for sufficiently small $h > 0$. Note that $||\phi_h(y_h)||_\infty$ approaches zero as $h \to 0$ since $||y_h||_\infty = 1$. Hence, if $h/\alpha_h \to 0$ as $h \to 0$, then $||v_h||_\infty \to 0$ as $h \to 0$, violating the condition $1 \le c||v_h||_\infty$. Therefore, h/α_h cannot approach zero and is bounded away from zero, i.e., there exists $\gamma > 0$ such that $h/\alpha_h \ge 1/\gamma$ for all small $h > 0$.

Finally, by the Taylor series expansion,

$$\psi'(x_h) = \psi'(0) + \psi''(0)x_h + O(h^2) = 1 + O(h^2),$$

where we noted that

$$\psi'(0) = 1, \quad \psi''(0) = 0, \quad ||x_h||_\infty = \alpha_h = O(h).$$

It then follows that

$$\begin{aligned} &\frac{1}{h}\Big(\psi'(x_h(t)) - \frac{1}{T}\int_0^T \psi'(x_h(t)dt\Big) \\ &= \frac{1}{h}\Big(1 + O(h^2) - \frac{1}{T}\int_0^T \big(1 + O(h^2)\big)dt\Big) \to 0 \end{aligned}$$

as $h \to 0$.

■

B. Proof of Theorem 2

We will prove stability of the linearized system (14) by showing that the average dynamics $\bar{A}$ is Hurwitz and the periodic perturbation $\mathscr{E}(t) := A(t) - \bar{A}$ is small. Since we consider the RIO control satisfying (11a), we shall regard (δ, h, μ, ϖ) as the design parameters instead of (g, h, μ, ϖ).

First, we show that $\bar{A}$ is Hurwitz in the limiting case where $\mu \to 1$ and $|h| \to 0$, provided (δ, ϖ) satisfies (17). Noting that $\bar{A}$ is given by $A(t)$ in (15) with $\psi'(x_d)$ replaced by $\kappa(x_d)$, the characteristic polynomial $p(\lambda) := \det(\lambda I - \bar{A})$ is obtained as

$$p(\lambda) = (\lambda^2 + c_1\lambda + \varpi^2)(\lambda^4 + c_2\lambda^3 + c_3\lambda^2 + c_4\lambda + c_5) \quad (27)$$

$$\begin{aligned} &c_1 := 2(2-\zeta)\varpi, \quad c_2 := 2\varpi\zeta + d_\alpha, \quad c_5 := k_\beta\varpi^2, \\ &c_3 := \varpi^2 + 2\varpi\zeta d_\alpha + k_\beta, \quad c_4 := \varpi^2 d_\alpha + 2k_\beta\varpi\zeta - \chi, \\ &\chi := (\delta/m)(\varpi^2 - \omega_d^2), \quad \zeta := 1 - \mu\kappa(x_d), \end{aligned}$$

where χ is expressed in terms of δ by solving (11a) for g and substituting the result to remove the explicit dependence of χ on g. Applying the Routh stability criterion, the characteristic polynomial with $\zeta = 0$ is Hurwitz if and only if

$$\varpi > 0, \quad d_\alpha > 0, \quad k_\beta > 0, \quad (28a)$$

$$\varpi^2 d_\alpha > \chi > -d_\alpha k_\beta, \quad \chi(\varpi^2 d_\alpha - d_\alpha k_\beta - \chi) > 0. \quad (28b)$$

It is tedious but straightforward to verify that condition (28b) is equivalent to (17). Thus, for the given (δ, ϖ), the characteristic polynomial with $\zeta = 0$ is Hurwitz. By continuity, there exists $\varepsilon > 0$ such that the original characteristic polynomial is Hurwitz for all ζ such that $|\zeta| < \varepsilon$. Let μ be chosen to satisfy $1 < \mu < 1 + \varepsilon$. Then $-\varepsilon < 1 - \mu < 0$ and hence $|\zeta| < \varepsilon$ if $\kappa(x_d)$ is sufficiently close to 1, which is the case when $|h|$ is sufficiently small for the following reason. In Lemma 2, $b_\mu(s)$ has no poles on the imaginary axis if and only if $\mu \neq 1$ when $b(s)$ is given by (8). Hence, when $|h|$ is sufficiently small, there exists a T-periodic solution $x_d(t)$ to (10) with its peak value $\|x_d\|_\infty$ converging to zero as $|h| \to 0$. In this case, $\kappa(x_d)$ approaches 1 as $|h|$ approaches zero. Thus stability of the average dynamics dictated by $\bar{A}$ is proven.

We now show that $\|\mathscr{E}\|_\infty$ approaches 0 as $|h| \to 0$. Let us denote x_d by x_h to show its dependence on h explicitly. There are only two nonzero entries of $\mathscr{E}(t)$, which are

$$\mathscr{E}_{24} := \frac{\chi l^\intercal}{4\varpi} \cdot \frac{\psi'(x_h) - \kappa(x_h)}{h} \cdot \frac{1}{\kappa(x_h)}$$

for the (2,4) entry and

$$\mathscr{E}_{44} := 2\varpi L(\psi'(x_h) - \kappa(x_h))$$

for the (4,4) entry. From Lemma 2,

$$\lim_{h\to 0} \mathscr{E}_{24} = \frac{\chi l^\intercal}{4\varpi} \cdot 0 \cdot 1 = 0$$

$$\lim_{h\to 0} \mathscr{E}_{44} = 2\varpi L \cdot 0 = 0.$$

Thus we have $\|\mathscr{E}\|_\infty \to 0$ as $h \to 0$.

C. System identification of the experimental test rig

The models of the motor electromagnetics E, motor-gear-arm G, and fluid load D in Fig. 10 are obtained by multiple experiments for system identification with ARX model described in [35]. For the identification purpose, we considered the closed-loop system in Fig. 12, where the feedback control from $\dot{z}$ to w through the RIO in Fig. 10 was replaced by a simple controller $L(s) = 0.045$.

We started with identifying the combined EG dynamics, where the control $L(s)$, the physical load D, and input v were removed from Fig. 12, and a chirp signal w was applied to E while the output $\dot{z}$ of G was measured and recorded. The chirp signal frequency was gradually increased from $2\pi/50$ rad/s to 50 rad/s. The input-output data $(w, \dot{z})$ was fit by a 6th order transfer function to obtain $G_m E_m(s)$.

We then closed the feedback loop by $w = L(s)z$ with the load still absent ($D = 0$). A human manually applied arbitrary pulsing torque v to this system and moved the robotic arm in an arbitrary manner. The input v and output $\dot{z}$ were fit by a 6th order transfer function $H(s)$. A model for the motor-gear-arm system is then obtained as $G_m(s) = H(s)(1 - L(s)G_m E_m(s))$, and a model for the motor electromagnetics is given by $E_m(s) = G_m E_m(s)/G_m(s)$.

We again substituted the controller as $L(s) = 1$ and repeated the system identification of the closed-loop system and obtained $\mathcal{H}(s)$. Finally, the physical fluid load D was attached to the closed-loop system as in Fig. 12, and a human applied arbitrary torque input v again. With the measured input $v(t)$ and output $\dot{z}(t)$, another transfer function $F(s)$ was obtained through a curve fit. A model for the load is then obtained by solving $F(s) = \mathcal{H}(s)/(1 - \mathcal{H}(s)D_m(s))$ for $D_m(s)$.

The models $E_m(s)$, $G_m(s)$ and $D_m(s)$ are of high order, and were reduced using balanced truncation [36] and an approximation of the frequency response. The simplified models were obtained as in (23).

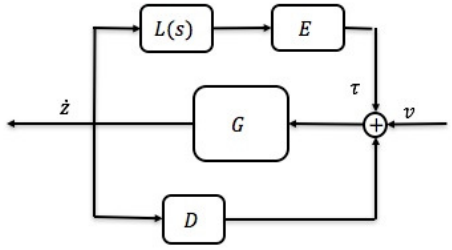

Fig. 12: Closed-loop setup for system identification

REFERENCES

[1] H. I. Krebs, N. Hogan, M. L. Aisen, and B. T. Volpe, "Robot-aided neurorehabilitation," *IEEE transactions on rehabilitation engineering*, vol. 6, no. 1, pp. 75–87, 1998.

[2] K. Suzuki, G. Mito, H. Kawamoto, Y. Hasegawa, and Y. Sankai, "Intention-based walking support for paraplegia patients with robot suit hal," *Advanced Robotics*, vol. 21, no. 12, pp. 1441–1469, 2007.

[3] L. Marchal-Crespo and D. J. Reinkensmeyer, "Review of control strategies for robotic movement training after neurologic injury," *Journal of neuroengineering and rehabilitation*, vol. 6, no. 1, p. 20, 2009.

[4] D. Sanz-Merodio, M. Cestari, J. C. Arevalo, and E. Garcia, "Control motion approach of a lower limb orthosis to reduce energy consumption," *International Journal of Advanced Robotic Systems*, vol. 9, no. 6, p. 232, 2012.
[5] C. Gosselin, T. Laliberté, B. Mayer-St-Onge, S. Foucault, A. Lecours, D. Gao, and R. Menassa, "A friendly beast of burden: A human-assistive robot for handling large payloads," *IEEE Robotics & Automation Magazine*, vol. 20, no. 4, pp. 139–147, 2013.
[6] G. Rosati Papini and C. A. Avizzano, "Transparent force control for body extender," in *IEEE RO-MAN*, pp. 138–143, IEEE, 2012.
[7] J. Rosen, M. Brand, M. B. Fuchs, and M. Arcan, "A myosignal-based powered exoskeleton system," *Systems, Man and Cybernetics, Part A: Systems and Humans, IEEE Transactions on*, vol. 31, no. 3, pp. 210–222, 2001.
[8] C. Fleischer and G. Hommel, "Emg-driven human model for orthosis control," in *Human Interaction with Machines*, pp. 69–76, Springer, 2006.
[9] A. B. Zoss, H. Kazerooni, and A. Chu, "Biomechanical design of the berkeley lower extremity exoskeleton (bleex)," *IEEE/ASME Transactions On Mechatronics*, vol. 11, no. 2, pp. 128–138, 2006.
[10] G. Cheron, M. Duvinage, C. De Saedeleer, T. Castermans, A. Bengoetxea, M. Petieau, K. Seetharaman, T. Hoellinger, B. Dan, T. Dutoit, *et al.*, "From spinal central pattern generators to cortical network: integrated bci for walking rehabilitation," *Neural plasticity*, vol. 2012, 2012.
[11] G. Orlovsky, T. Deliagina, and S. Grillner, *Neuronal control of locomotion: from mollusc to man*. Oxford University Press, 1999.
[12] L. Righetti and A. Ijspeert, "Programmable central pattern generators: an application to biped locomotion control," *Proc. IEEE Int. Conf. Robotics and Automation*, pp. 1585–1590, 2006.
[13] N. L. Tagliamonte, F. Sergi, G. Carpino, D. Accoto, and E. Guglielmelli, "Human-robot interaction tests on a novel robot for gait assistance," in *Rehabilitation Robotics (ICORR), 2013 IEEE International Conference on*, pp. 1–6, IEEE, 2013.
[14] R. Ronsse, T. Lenzi, N. Vitiello, B. Koopman, E. van Asseldonk, S. M. M. De Rossi, J. van den Kieboom, H. van der Kooij, M. C. Carrozza, and A. J. Ijspeert, "Oscillator-based assistance of cyclical movements: model-based and model-free approaches," *Medical & biological engineering & computing*, vol. 49, no. 10, p. 1173, 2011.
[15] T. Matsubara, A. Uchikata, and J. Morimoto, "Full-body exoskeleton robot control for walking assistance by style-phase adaptive pattern generation," in *Intelligent Robots and Systems (IROS), 2012 IEEE/RSJ International Conference on*, pp. 3914–3920, IEEE, 2012.
[16] D. Papageorgiou and Z. Doulgeri, "A kinematic controller for human-robot handshaking using internal motion adaptation," in *2015 IEEE International Conference on Robotics and Automation (ICRA)*, pp. 5622–5627, May 2015.
[17] T. Iwasaki, J. Chen, and W. O. Friesen, "Biological clockwork underlying adaptive rhythmic movements," *Proceedings of the National Academy of Sciences*, vol. 111, no. 3, pp. 978–983, 2014.
[18] T. Iwasaki and M. Zheng, "Sensory feedback mechanism underlying entrainment of central pattern generator to mechanical resonance," *Biological cybernetics*, vol. 94, no. 4, pp. 245–261, 2006.
[19] Y. Futakata and T. Iwasaki, "Formal analysis of resonance entrainment by central pattern generator," *J. Math. Biol.*, vol. 57, no. 2, pp. 183–207, 2008.
[20] Y. Futakata and T. Iwasaki, "Entrainment to natural oscillations via uncoupled central pattern generators," *IEEE Trans. Auto. Contr.*, vol. 56, no. 5, pp. 1075–1089, 2011.
[21] M. Desmurget and S. Grafton, "Forward modeling allows feedback control for fast reaching movements," *Trends in cognitive sciences*, vol. 4, no. 11, pp. 423–431, 2000.
[22] T. E. Milner, "A model for the generation of movements requiring endpoint precision," *Neuroscience*, vol. 49, no. 2, pp. 487–496, 1992.
[23] S. W. Keele, "Behavioral analysis of movement," *Comprehensive Physiology*, 1981.
[24] G. Hinton, "Parallel computations for controlling an arm," *Journal of motor behavior*, vol. 16, no. 2, pp. 171–194, 1984.
[25] J. R. Flanagan, D. J. Ostry, and A. G. Feldman, "Control of trajectory modifications in target-directed reaching," *Journal of motor behavior*, vol. 25, no. 3, pp. 140–152, 1993.
[26] R. Grush, "The emulation theory of representation: Motor control, imagery, and perception," *Behavioral and brain sciences*, vol. 27, no. 03, pp. 377–396, 2004.
[27] H. Miyamoto, M. Kawato, T. Setoyama, and R. Suzuki, "Feedback-error-learning neural network for trajectory control of a robotic manipulator," *Neural networks*, vol. 1, no. 3, pp. 251–265, 1988.
[28] J. Zhao and T. Iwasaki, "CPG control for assisting human with periodic motion tasks," in *2016 IEEE 55th Conference on Decision and Control (CDC)*, pp. 5035–5040, Dec 2016.
[29] R. Seidler, D. Noll, and G. Thiers, "Feedforward and feedback processes in motor control," *Neuroimage*, vol. 22, no. 4, pp. 1775–1783, 2004.
[30] D. A. Rosenbaum, *Human motor control*. Academic press, 2009.
[31] H. Khalil, *Nonlinear Systems*. Prentice Hall, 1996.
[32] T. Iwasaki, "Multivariable harmonic balance for central pattern generators," *Automatica*, vol. 44, no. 12, pp. 3061–3069, 2008.
[33] R. Bellman, *Stability theory of differential equations*. Courier Corporation, 2013.
[34] L. Baratchart, M. Chyba, and J.-B. Pomet, "A Grobman-Hartman theorem for control systems," *Journal of Dynamics and Differential Equations*, vol. 19, no. 1, pp. 75–107, 2007.
[35] L. Ljung, "System identification," in *Signal analysis and prediction*, pp. 163–173, Springer, 1998.
[36] B. Moore, "Principal component analysis in linear systems: Controllability, observability, and model reduction," *IEEE transactions on automatic control*, vol. 26, no. 1, pp. 17–32, 1981.

Jinxin Zhao received his B.S. degree in Mechanical Engineering from Zhejiang University, China in 2011, his M.S. degree in Aerospace Engineering from University of Michigan, Ann Arbor in 2013 and his Ph.D. degree from the Department of Mechanical and Aerospace Engineering, University of California, Los Angeles. He is currently working as Research Scientist at Baidu Research Institute. His research interests include vehicle control and system identification, adaptive human-robot interactive control and distributed control of microgrid.

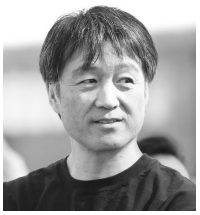

Tetsuya Iwasaki (M'90-SM'01-F'09) received his B.S. and M.S. degrees in Electrical and Electronic Engineering from the Tokyo Institute of Technology (Tokyo Tech) in 1987 and 1990, respectively, and his Ph.D. degree in Aeronautics and Astronautics from Purdue University in 1993. He held a Post-Doctoral Research Associate position at Purdue University (1994-1995), and faculty positions at Tokyo Tech (1995-2000) and at the University of Virginia (2000-2009), before joining the UCLA faculty as Professor of Mechanical and Aerospace Engineering. Dr. Iwasaki's current research interests include dynamics and control of animal locomotion, coupled nonlinear oscillators, global pattern formation via local interactions, and robust/optimal control theories and their applications to engineering systems. He has received CAREER Award from NSF, Pioneer Prize from SICE, George S. Axelby Outstanding Paper Award from IEEE, Rudolf Kalman Best Paper Award from ASME, and Steve Hsia Biomedical Paper Award at the 8th World Congress on Intelligent Control and Automation. He has served as Associate Editor of *IEEE Transactions on Automatic Control*, *Systems & Control Letters*, *IFAC Automatica*, *International Journal of Robust and Nonlinear Control*, and *SIAM Journal on Control and Optimization*.